Thermoresponsive Water Transportation in Dually Electrostatically Crosslinked Nanocomposite Hydrogels

Heqin Huang, Yang Yang, Xiaojie Wang, Florian Rehfeldt, and Kai Zhang*

Controlling water transportation within hydrogels makes hydrogels attractive for diverse applications, but it is still a very challenging task. Herein, a novel type of dually electrostatically crosslinked nanocomposite hydrogel showing thermoresponsive water absorption, distribution, and dehydration processes are developed. The nanocomposite hydrogels are stabilized via electrostatic interactions between negatively charged poly(acrylic acid) and positively charged layered double hydroxide (LDH) nanosheets as well as poly(3-acrylamidopropyltrimethylammonium chloride). Both LDH nanosheets as crosslinkers and the surrounding temperatures played pivotal roles in tuning the water transportation within these nanocomposite hydrogels. By changing the surrounding temperature from 60 to 4 °C, these hydrogels showed widely adjustable swelling times between 2 and 45 days, while the dehydration process lasted between 7 and 27 days. A swift temperature decrease, for example, from 60 to 25 °C, generated supersaturation within these nanocomposite hydrogels, which further retarded the water transportation and distribution in hydrogel networks. Benefiting from modified water transportation and rapidly alternating water uptake capability during temperature change, pre-loaded compounds can be used to track and visualize these processes within nanocomposite hydrogels. At the same time, the discharge of water and loaded compounds from the interior of hydrogels demonstrates a thermoresponsive sustained release process.

Synthetic hydrogels are formed with crosslinked hydrophilic polymer chains and often have highly porous and heterogeneous microstructure.[1] These features endow the hydrogels with excellent water uptake capability and allow rapid water transportation in hydrogels.[2] For the treatment of industry waste water, hydrogels can be used to absorb and accumulate heavy metal ions and dyes from aqueous solutions.[3] Furthermore, hydrogels are often considered ideal materials for biomedical engineering.[4] Hydrophilic drug, nutrient, and waste can be transported along with water, which endow hydrogels with great potential for drug release devices[5] or scaffold materials for cells and tissue culture.[6]

Since water is a critical component of hydrogels, one would reasonably regulate the functions of hydrogels by tuning water contents[7–9] and controlling water transportation.[10–13] However, it is still extremely challenging to manipulate the movement of water in artificial hydrogels.[14] The water transportation is largely affected by polymer hydrophilicity and hydrogel microstructures, which are strongly affected by the hydrogel composition and the preparation method.[15] Dense hydrogel networks can be prepared by increasing the crosslinking density, which leads to reduced average molecular weight between crosslinkers and therefore retarded water penetration in denser polymer network.[11] In comparison, excessive crosslinkers lead to phase separation and form highly heterogeneous microstructure, and therefore undermine the water preserve capability of hydrogels.[16,17] In another way, thermoresponsive hydrogels with poly(N-isopropylacrylamide) largely shrinks with the surrounding temperature exceeding its lower critical solution temperature of around 32 °C, while hydrophilic hydrogel polymer networks become hydrophobic.[18,19] Such shrinking process causes spontaneous water loss of hydrogels due to fast phase transition of polymer chains and generally fails in the more delicate control of water transport within hydrogels.[20] Thus, even when it is well known that microstructures and hydrophilicity of hydrogel networks are critical to regulate the water transportation, it is still difficult to continuously control the speed of water absorption, distribution, and discharge in synthetic hydrogels.

Herein, a novel kind of nanocomposite hydrogels was prepared to achieve controllable and stimuli-responsive water transportation. These hydrogels contained dually crosslinked dense polymer networks and low water content (28.7% at 25 °C), but still maintained the uniform microstructures for water transportation in the hydrogels. More importantly, ultimate swelling

Dr. H. Huang, Dr. Y. Yang, X. Wang, Prof. K. Zhang
Wood Technology and Wood Chemistry
University of Goettingen
Büsgenweg 4, D-37077 Göttingen, Germany
E-mail: kai.zhang@uni-goettingen.de
Dr. F. Rehfeldt
Third Institute of Physics–Biophysics
Faculty of Physics
University of Goettingen
Friedrich-Hund-Platz 1, D-37077 Göttingen, Germany

ratios, which was defined herein as the weight ratio of fully swollen hydrogels and dried hydrogels, and water transportation speeds in nanocomposite hydrogels can be continuously adjusted by changing the surrounding temperature. Water transportation was largely retarded, while the equilibrium swelling ratio of hydrogels was adjusted within a few seconds by changing temperature. This distinction provided a unique opportunity to observe the water distribution and discharge in supersaturated hydrogels with temporal phase separation regions, for example, by tracking the release of loaded rhodamine B (RhB) molecules. In particular, these dually crosslinked nanocomposite hydrogels showed water preserve functions and can serve as sustained and thermoresponsive delivery system.

LDH nanosheets were obtained with a diameter of ≈45 nm and thickness of ≈2 nm (**Figure 1**a,b). Because of the highly positive zeta potential (> +40 mV) and layered structure, LDH nanosheets were exfoliated by acrylic acid and showed excellent dispersion in water (Figure S1, Supporting Information). For a typical recipe of Gel-A-1.25, the precursor contained 1.25 wt% LDH nanosheets, 25 vol% acrylic acid, and 0.5 wt% photoinitiator

I2959. The pH value of LDH suspension was measured as 9.1, which originated from the weak ionization of LDH nanosheets. This weak basic suspension promoted the protonation of AAc and, therefore, led to effective crosslinking. Furthermore, the precursor of Gel-A-1.25, including LDH nanosheets, AAc, and I2959, showed pH value as 2.7, which indicated excessive AAc in Gel-A-1.25. After the first polymerization, Gel-A-1.25 was mainly crosslinked by the electrostatic interactions between LDH nanosheets and poly(acrylic acid) (PAAc) (Figure 1c). Resulting hydrogel Gel-B-1.25 after the second polymerization not only included nanocrosslinking via LDH nanosheets, but also involved the interactions between polyanionic PAAc and polycationic poly(3-acrylamidopropyltrimethylammonium chloride) (PAPTMAC) (Figure 1d). Because of distinct crosslinking densities, water content of Gel-A-1.25 lay at ≈78.3%, while Gel-B-1.25 had only ≈28.7% water. In Gel-B, ionized PAAc and PAPTMAC chains with opposite charges largely occupied the hydrophilic groups of each other. Therefore, Gel-B-1.25 specimens largely shrunk in volume during the soaking process and eventually reached a lower water content compared to their precursors.
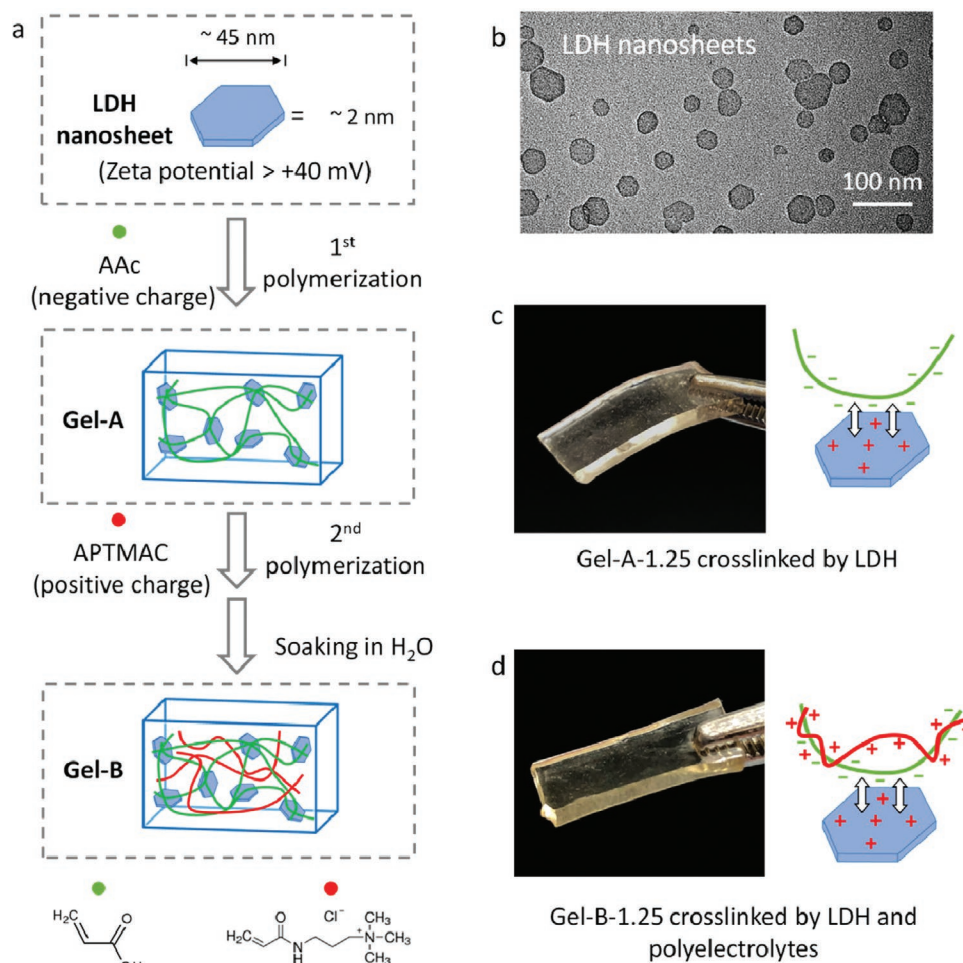

Figure 1. Preparation and composition of Gel-A and Gel-B via dual electrostatic crosslinking. a) Schematic illustration for the preparation of Gel-A and Gel-B. b) TEM images of LDH nanosheets. c) Photo of Gel-A-1.25 and schematic illustration for the PAAc-LDH nanosheets crosslinking mechanism. d) Photo of Gel-B-1.25 and schematic illustration for dual crosslinking with LDH nanosheets and polyelectrolytes. AAc, acrylic acid; APTMAC, 3-acrylamidopropyltrimethylammonium chloride.

In addition, the ultimate swelling ratios were identical in Gel-B-1.25 with different thickness, although the swelling process was delayed in the thicker hydrogels. As shown in Figure S2, Supporting Information, Gel-B-1.25 specimens has identical length and width of 4.5 mm but various thicknesses of 1.5, 3, and 4.5 mm. These hydrogels with distinct thicknesses showed nearly the same equilibrium swelling ratios after 5 days, which indicated identical compositions of these hydrogels.

The contributions of dually electrostatic interactions between PAAc/LDH nanosheets and PAAc/PAPTMAC were further investigated using mechanical tests. LDH nanosheets acted as nanocrosslinkers within Gel-A by generating soft and elastic hydrogels with G′ = 5670 Pa at a frequency of 0.1 rad s^{-1} (**Figure 2**a). With the presence of dually electrostatic crosslinking, Gel-B-1.25 became stiffer (G′ = 8660 Pa at a frequency of 0.1 rad s^{-1}) and in particular more viscous in the high frequency region (with tan δ approaching 0.81 at a frequency of 100 rad s^{-1}). This fact is predominantly because of electrostatic interactions generated between polyelectrolyte chains in addition to already existing electrostatic interactions between PAAc and LDH nanosheets. Under 60% compression, Gel-B-1.25 not only showed 2.86 times greater compression stress as that of Gel-A-1.25, but also had ≈5.23 times larger hysteresis area in the loading–unloading cycles (Figure 2b).

Furthermore, LDH nanosheets as nanocrosslinkers provided additional multiple functionality including mechanical enhancement,[21,22] so that Gel-A-1.25 and Gel-B-1.25 both showed little change in the first three hysteresis cycles and demonstrated outstanding structural stability. At the same time, Gel-A-1.25 and Gel-B-1.25 both had ultimate elongation ratios greater than 5, but distinct tensile stress. Gel-B-1.25 had an ultimate tensile stress of up to ≈1.38 MPa, when the gels were stretched to five times their original length. In comparison, the maximal tensile stress of Gel-A-1.25 was only about 0.35 MPa at an equal elongation ratio (Figure 2c). In tearing tests (Figure S3, Supporting Information), both Gel-A-1.25 and Gel-B-1.25 exhibited significant resistance against the crack propagation showing their high mechanical toughness, while Gel-B-1.25 specimens were much tougher than Gel-A-1.25.[23]

In addition to these advantageous mechanical properties of Gel-B, their interior microstructures were strongly affected by the dosage of LDH nanosheets. As-prepared Gel-A specimens with diverse amounts of LDH nanosheets were all transparent. In

comparison, Gel-B with LDH nanosheets of 0.6 wt% and 0.3 wt% became opaque after the soaking process (**Figure 3**a). With higher amount of LDH nanosheets of 1.25 wt%, equilibrated Gel-B specimens were transparent. These different transparencies should be ascribed to distinct microstructures that were slowly stabilized during the soaking process (Figure S4, Supporting Information). Freeze-dried Gel-B-1.25 had dense polymer networks and nearly no microsized pores. In contrast, freeze-dried Gel-B-0.3 exhibited a highly porous and interconnected microstructure. This structural difference indicates that a sufficiently high amount of LDH nanosheets was necessary to maintain uniform hydrogel networks during the soaking process.[24,25] The highly porous microstructures in the Gel-B with less LDH nanosheets reasonably led to greater swelling ratios. In 25 °C water, Gel-B-1.25 had a swelling ratio of ≈139.5%. In comparison, the porous microstructure in opaque hydrogels Gel-B-0.6 and Gel-B-0.3 was favorable in absorbing more water, with swelling ratios of ≈142.8% for Gel-B-0.6 and ≈165.2% for Gel-B-0.3 (Figure 3b).

As well, these different microstructures due to distinct contents of LDH nanosheets largely affected the water transportation from the interior to the outside of hydrogels and vice versa. Comparing with Gel-B-0.6 and Gel-B-0.3, Gel-B-1.25 dried more slowly during the dehydration process in air with 50% relative humidity (rh) at 25 °C (Figure 3c). Even though Gel-B-1.25 had the smallest water contents (≈28.7 wt%) at the fully swollen state, Gel-B-1.25 preserved the most water (≈18.6 wt%) after the first 8 h of drying. Under the same condition, the water contents of Gel-B-0.6 reduced from ≈29.9% to ≈17.7% within the first 7 h, and those of Gel-B-0.3 decreased from ≈39.3% to ≈17.7%. In the Gel-B with lower amounts of LDH nanosheets, a larger fraction of water was stored in their porous structures as free water and could thus be transported faster out of the hydrogels, causing faster water loss within the first 8 h. In the following long-time drying process (Figure 3c), the water contents of all hydrogels became stable after about 10 days. Eventually, the water content of Gel-B-1.25 was ≈10.4% after 14 days of dehydration process, while water remained in Gel-B-0.6 and Gel-B-0.3 had a mass fraction of ≈8.9% and ≈7.0%, respectively. Therefore, the dense microstructure in Gel-B induced by high amounts of LDH nanosheets not only retarded the water loss, but also improved the water preservation of hydrogels.

In addition to porous microstructures, surrounding temperatures also affected the swelling process of Gel-B-1.25 (Figure 3d).
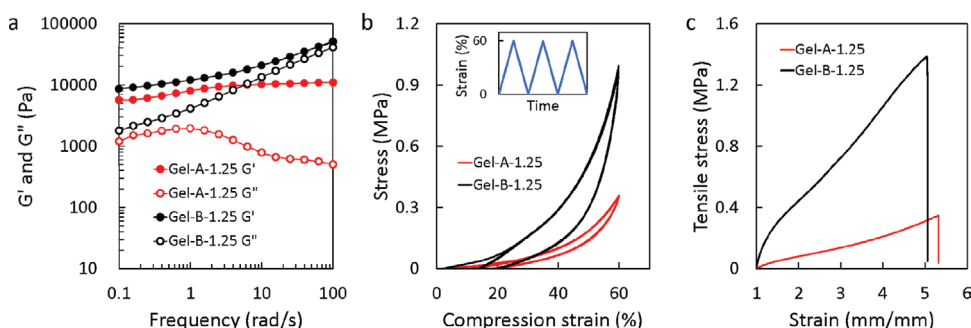

Figure 2. Mechanical properties of Gel-A-1.25 and Gel-B-1.25. a) Oscillation shear frequency sweep of hydrogels. b) The compression loading–unloading stress–strain curves of hydrogels. The inset shows continuous loading-unloading deformation with the strain of 60%. c) Tensile stress–strain curves of hydrogels.
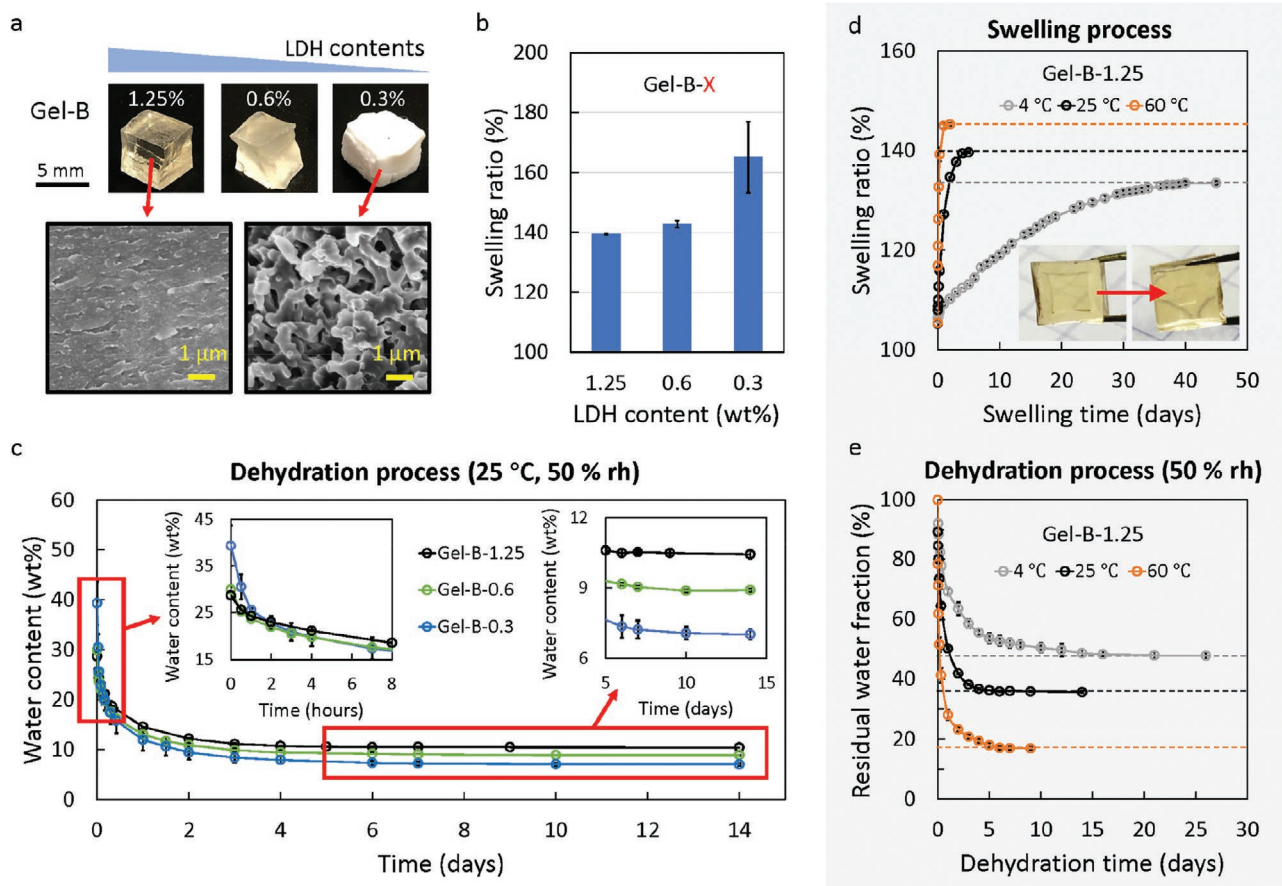
**ADVANCED
SCIENCE NEWS**
www.advancedsciencenews.com

**Macromolecular
Rapid Communications**
www.mrc-journal.de

Figure 3. Dehydration behaviors and swelling behaviors of Gel-B. a) Microstructure changes of Gel-B specimens with diverse contents of LDH nanosheets. b) Swelling ratios of Gel-B specimens with various contents of LDH nanosheets at 25 °C. X is 1.25, 0.6, or 0.3. c) Water contents of diverse Gel-B specimens during the dehydration process in the air with 50% relative humidity at 25 °C. d) Swelling process and e) dehydration process of Gel-B-1.25 at 4, 25, and 60 °C.

In 60 °C water, the swelling process of Gel-B-1.25 finished within ≈2 days with ultimate swelling ratios of ≈145.3%. In comparison, lower swelling temperatures led to much longer swelling duration and lower swelling ratios. At 25 °C, the full swelling of Gel-B-1.25 required ≈5 days with swelling ratios of ≈139.6%, while the swelling process at 4 °C took as long as 45 days with swelling ratios of ≈133.5%. As shown in Figure 3d, fully hydrated polymer networks and the areas that are not yet fully swollen have different refractive indexes. Therefore, a visible core in hydrogels was visible during the swelling process and shrank continuously, until it completely disappeared and the whole hydrogel became fully swollen.

The dehydration process of hydrogels was highly retarded and largely affected by the temperature. At 4 °C, Gel-B-1.25 maintained ≈47.8% water in the swollen state after 4 weeks of exposure to the surroundings of 50% rh (Figure 3e). At 25 °C and 50% rh, ≈35.7% of water was preserved, while only 16.9% of water was kept after 1 week at 60 °C and 50% rh. In particular, the final water content in these Gel-B specimens maintained even after longer exposure to the same surroundings and did not dry out. Thus, the water preservation capability of Gel-B-1.25 can also be regulated by varying the surrounding temperature. The thermal-sensitive water preservation should

be predominantly attributed to the partially ionization of PAAc. Increasing temperature generally promotes the ionization of water,[26] which weakens the electrostatic interaction between PAAc/LDH nanosheets or PAAc/PAMPTAC and enhances the water absorption. A similar phenomenon was visible, when Gel-B-1.25 was swollen in aqueous NaCl solution. Improved ionic strength also weakened the electrostatic crosslinking in hydrogels and promoted the equilibrium swelling ratio (Figure S5, Supporting Information).[27]

Furthermore, the nanocrosslinking via LDH nanosheets should have provided critical contribution for preserving water and retarding water loss. As comparison, LDH nanosheets were replaced by covalent crosslinker N,N′-methylenebis(acrylamide) (0.25 or 0.5 mol% of the amount of AAc) to prepare covalently crosslinked Gel-B-C0.25 and Gel-B-C0.5. Swelling ratios of these chemically crosslinked hydrogels only showed neglectable changes at diverse temperatures (Figure S6a, Supporting Information). The covalently crosslinked Gel-B-C0.25 and Gel-B-C0.5 had greater equilibrium swelling ratios of >170% because the static covalent crosslinking had limited their shrinking during the soaking process. Therefore, the network within the dynamic Gel-B hydrogels stabilized by the electrostatic crosslinking between PAAc/LDH nanosheets and PAAc/PAPTMAC should

**ADVANCED
SCIENCE NEWS**

www.advancedsciencenews.com

**Macromolecular
Rapid Communications**

www.mrc-journal.de

have been rearranged during the soaking process and generated denser hydrogel networks with less water. For covalently crosslinked hydrogels, only increasing the concentration of crosslinkers will generate permanent phase separation in the primary hydrogel network (normally with a ratio of crosslinkers to monomer >1 mol%), which will cause adverse effects. Furthermore, the polyelectrolyte chains should have been highly condensed around LDH nanosheets due to their large size compared to polymer chains and highly positive surface charge. Therefore, the electrostatic crosslinking networks will be weakened with rising surrounding temperature. The weaker interactions promote the water uptake of Gel-B specimens and drive their volume expansion.[28]

The formation of such supersaturated network by decreasing the temperature was even clearly visible. Fully swollen dynamic

Gel-B-1.25 in 60 °C water became opaque within a few seconds, when it was transferred into 25 °C water (**Figure 4**a). The spontaneous decrease of temperature induced only very slight shrinking of hydrogels. On the contrary, the accompanying water loss of only few weight percents lasted for several days. This supersaturated state of hydrogels also existed in Gel-B-C0.25 and Gel-B-C0.5, but much less obvious (Figure S6b, Supporting Information). Therefore, the presence of both dynamic electrostatic crosslinking allowing the rearrangement of the network components and the formation of dense structures around LDH nanosheets should be the primary reasons for the swift transparency change. Nevertheless, this modified hydrogel network highly retarded water loss and prevented the rapid water transportation to the outside by locking water within hydrogels. Only a slight decrease of water content (of ≈5.7%)
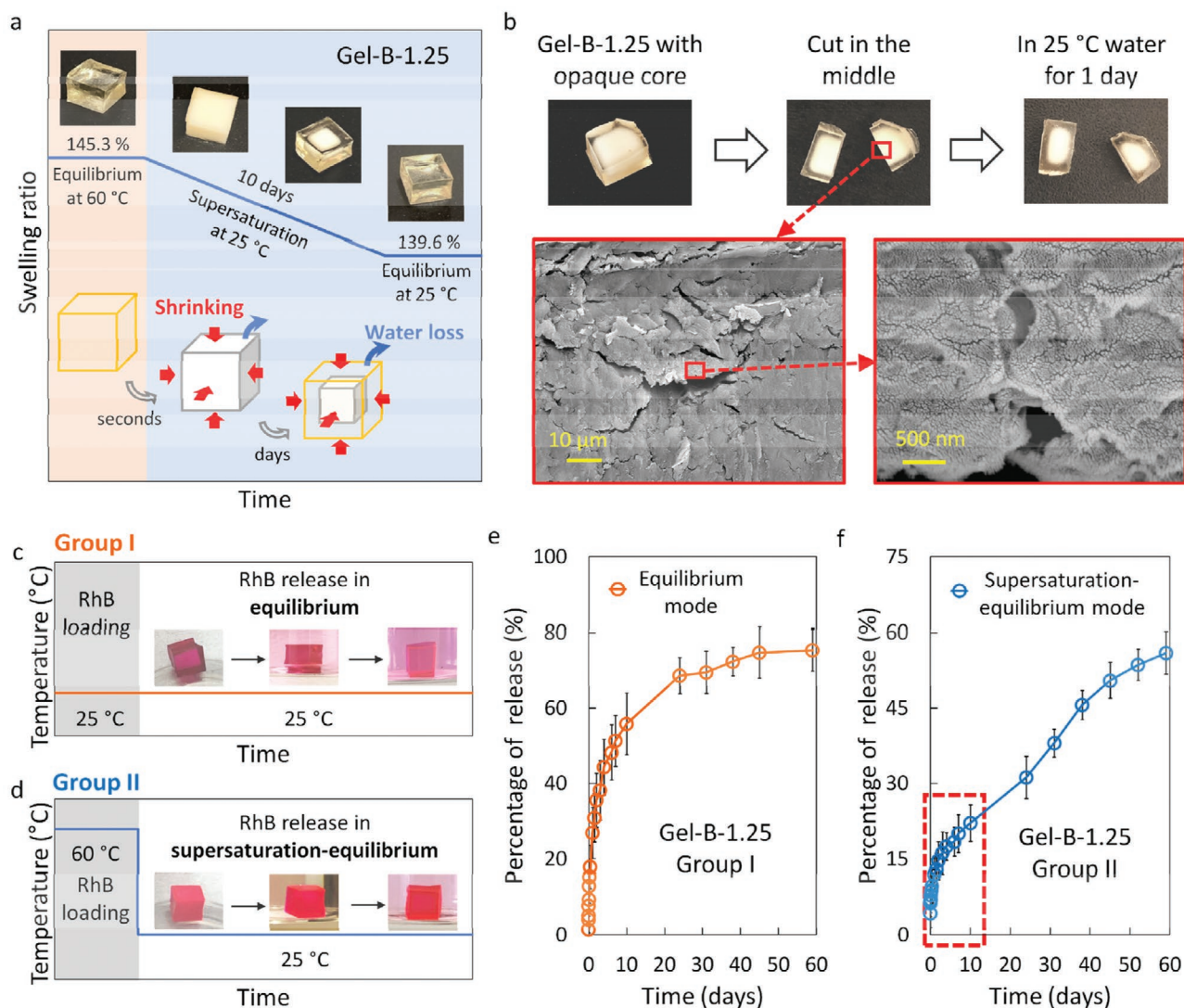

Figure 4. Supersaturation in Gel-B-1.25. a) Change of Gel-B-1.25 by transferring hydrogels from 60 °C water to 25 °C water and schematic illustration for the slow dissipation of supersaturation state in hydrogels. b) The dissipation of opaque zone in the cut Gel-B-1.25 and SEM images of the opaque zone. c) RhB release in the equilibrium state (group I). d) RhB release in the supersaturation–equilibrium state (group II). e,f) Release curves of RhB during the equilibrium mode and supersaturation–equilibrium mode from Gel-B-1.25 in group I and group II, respectively. The red dashed box in (f) indicates the accelerated release in the first 10 days.

**ADVANCED
SCIENCE NEWS**

www.advancedsciencenews.com

**Macromolecular
Rapid Communications**

www.mrc-journal.de

was finally observed. Since Gel-B-1.25 has a slightly higher swelling ratio (≈145.3%) at 60 °C than at 25 °C (≈139.6%), the excess water in the hydrogels were spontaneously released from bound sites and underwent a temporary phase separation forming the opaque structure. The dissipation of this opaque structure required about 10 days at 25 °C, until Gel-B-1.25 reached the equilibrium state and became transparent again (Figure 4a). Dried opaque regions demonstrated shrunk and wrinkled microstructure of original hydrogels (Figure 4b). The released excess water was obviously discharged at the hydrogel surface. Therefore, the opaque regions containing inversely supersaturated water molecules in the matrix generated a new transparent shell after 1 day of immersion in water (Figure 4b). Therefore, this reversible change of transparency was due to a temporal supersaturation of water molecules within Gel-B, which formed inhomogeneous polymer networks and further retarded the water distribution within hydrogels.

Moreover, the long duration for the regeneration of homogeneous hydrogels allowed us to observe the slow transformation between the equilibrium states at diverse temperatures as well as by the intermediate states between these equilibrium states. Since the regeneration of the equilibrium state for the uniform hydrogel was a delayed water transportation process, this process can be tracked using water-soluble molecules. In the present study, RhB was used as a hydrophilic model molecule to further observe the water transportation in our hydrogels. In group I (Figure 4c), dried Gel-B-1.25 was immersed in aqueous RhB solution (0.1 mg mL^{-1}) at 25 °C until fully swollen to load RhB, before RhB was released in 25 °C water. In group II (Figure 4d), the RhB was loaded into the Gel-B-1.25 with the same method but at 60 °C, while the release of RhB was conducted at 25 °C. A higher loading temperature reasonably led to a higher loading capability, and RhB was loaded into hydrogels at 60 °C with an amount of ≈44.2 wt% of polymer weight. In comparison, RhB loaded in the same hydrogels at 25 °C in group I was only ≈15.3 wt% of polymer weight.

In group I, the same loading and release temperatures of 25 °C were applied, so that Gel-B-1.25 underwent an equilibrium release mode. The release of RhB was purely driven by the osmotic pressure (Figure 4e). With a high loading temperature of 60 °C and the same release temperature of 25 °C, the RhB release in group II started with a supersaturated state in hydrogels immediately after the temperature change. As shown in Figure 4d, once hydrogels were transferred from 60 °C into 25 °C water, the Gel-B in group II became opaque immediately and got slowly transparent again in roughly 10 days. The process for the opaque–transparent transition with accompanying release of RhB was marked by a dash box in Figure 4f. Comparing hydrogels in group I and group II, the release ratio of RhB from group I within the first 10 days was obviously higher, although the total released amount was much lower due to lower loaded amount of RhB in group I. The lower releasing ratio of RhB from hydrogels of group II within the first 10 days was due to the retarded water loss and thus a delayed water transport from the interior to the outside of hydrogels.

After the first 10 days, the release of RhB in group I hydrogels became slower and was largely delayed to ≈45 days due to the retarded water transportation to reach the plateau. In comparison, the hydrogels in group II became transparent with gradual dissipation of opaque core, and the release process in these hydrogels gradually changed into an equilibrium mode that is purely driven by the osmotic pressure. Thus, Gel-B-1.25 hydrogels in group II showed, in fact, a supersaturation–equilibrium release mode. The dissipation of the opaque core was intrinsically the same process to discharge extra water in hydrogels, and RhB molecules in the hydrogels in group II were discharged to surrounding water along with the loss of water. Comparing the release process within the first 10 days and afterward, the hydrogels in group II showed an accelerated release within the first 10 days. During this period, the release of RhB was not only driven by the osmotic pressure due to the concentration difference of RhB, but also accelerated by the pressure caused by the supersaturation process. Finally, 75.4% RhB was released from hydrogels of group I after 60 days, while 56.1% RhB was released from hydrogels of group II. The residual RhB in hydrogels of group II can be further released according to the equilibrium release mode at 25 °C, which demonstrates a sustained release of loaded compounds. Therefore, the water transportation process within nanocomposite hydrogels could be regulated by the temperature and tracked by using the water-soluble RhB molecules. Moreover, the thermosensitive release behaviors of pre-loaded molecules from the hydrogels can be realized via distinct release processes.

In conclusion, a novel type of dynamic nanocomposite hydrogels showing thermoresponsive water transportation was constructed through dual crosslinking via electrostatic interaction. In the dually crosslinked Gel-B-1.25, a dense microstructure largely delayed the water transportation and was favorable in preserving water during the dehydration process. The hydration and dehydration process were readily controllable by the surrounding temperature. At 60 °C, Gel-B had a large swelling ratio (≈145.3%) and the dehydration process of hydrogels took ≈7 days, which was as fast as regular hydrogels. At 25 °C and 4 °C, the same hydrogels had equilibrium swelling ratios of ≈139.6% and ≈133.5%, while the drying process took ≈14 days and ≈27 days, respectively. Furthermore, the temperature change caused rapid swelling and shrinking, while the water absorption and discharge process were largely retarded. This conflict led to phase separation within hydrogels during the temperature decrease and generated opaque network within hydrogels. The slow dissipation process of this non-transparent network provided a unique opportunity to observe the water transportation in the supersaturated hydrogels. In total, these dually crosslinked dynamic hydrogels showed thermosensitive water transportation behaviors. Such hydrogels and the strategy to control the water transportation within hydrogels can be further used to develop hydrogel devices with water-preserving functions or used for sustained and thermoresponsive drug delivery systems.

Experimental Section

Preparation of LDH Nanosheets: Mg$_2$Al-CO$_3$ LDH nanosheets were synthesized based on a previously described protocol.[29] Briefly, 80 mL of a basic aqueous solution of 0.15 M NaOH and 0.013 M Na$_2$CO$_3$ was mixed with 20 mL of a solution containing 2.0 mmol of MgCl$_2$ and 1.0 mmol of AlCl$_3$ under vigorous stirring. The obtained milky solution was sealed and continuously stirred for 10 min. The resultant mixture was then centrifuged (8000 rpm, 5 min) and washed with water three

times, and the resulting white slurry was dispersed in 80 mL of deionized (DI) water. The hydrothermal exfoliated process was subsequently carried out in a sealed flask at 95 °C for 4 h. A slightly blue colloid with a concentration of 0.4 wt% was finally obtained as the product.

Preparation of Gel-A and Gel-B: In a typical recipe for Gel-A-1.25, LDH nanosheet suspension of 2 wt% (500 µL), acrylic acid (200 µL), and photoinitiator I2959 (0.5 wt%) were mixed thoroughly. The total volume was adjusted to 800 µL, in which the content of LDH nanosheets was 1.25 wt%. After 30 min, the slightly blue LDH suspension became transparent and colorless (Figure S1, Supporting Information). This transparent precursor solution was purged with nitrogen gas for 5 min and exposed to UV irradiation for 4 h to form Gel-A-1.25. The soft and elastic Gel-A-1.25 was then immersed in the solution of APTMAC solution (15 wt%) containing 0.5 wt% I2959. After 7 days of swelling, the second polymerization was performed under UV irradiation for 4 h. Resulting Gel-B-1.25 was repeatedly soaked in hot water (80 °C) to remove the unreacted molecules in the hydrogels.

Loading and Release of RhB: RhB was loaded by immersing hydrogels in RhB solution (0.1 mg mL^{-1}) for 1 week. The loading amounts were determined by comparing concentrations of RhB of RhB solution before and after the loading process. The RhB release experiments were performed in 20 mL of DI water. For each detection time point, 1 mL of solution was used and the RhB concentration was determined using UV–vis spectroscopy.

Supporting Information

Acknowledgements

Conflict of Interest

The authors declare no conflict of interest.

Keywords

[1] Y. S. Zhang, A. Khademhosseini, *Science* **2017**, *356*, eaaf3627.
[2] E. A. Appel, J. del Barrio, X. J. Loh, O. A. Scherman, *Chem. Soc. Rev.* **2012**, *41*, 6195.
[3] G. Jing, L. Wang, H. Yu, W. A. Amer, L. Zhang, *Colloids Surf. A* **2013**, *416*, 86.
[4] A. M. Rosales, K. S. Anseth, *Nat. Rev. Mater.* **2016**, *1*, 15012.
[5] H. Huang, J. Xu, K. Wei, Y. J. Xu, C. K. Choi, M. Zhu, L. Bian, *Macromol. Biosci.* **2016**, *16*, 1019.
[6] N. Annabi, A. Tamayol, J. A. Uquillas, M. Akbari, L. E. Bertassoni, C. Cha, G. Camci-Unal, M. R. Dokmeci, N. A. Peppas, A. Khademhosseini, *Adv. Mater.* **2014**, *26*, 85.
[7] T. Verho, M. Karesoja, P. Das, L. Martikainen, R. Lund, A. Alegria, A. Walther, O. Ikkala, *Adv. Mater.* **2013**, *25*, 5055.
[8] M. Ilyas, M. A. Haque, Y. Yue, T. Kurokawa, T. Nakajima, T. Nonoyama, J. P. Gong, *Macromolecules* **2017**, *50*, 8169.
[9] S. Nakagawa, X. Li, H. Kamata, T. Sakai, E. P. Gilbert, M. Shibayama, *Macromolecules* **2017**, *50*, 3388.
[10] W. Hong, X. Zhao, Z. Suo, *J. Appl. Phys.* **2008**, *104*, 084905.
[11] T. Fujiyabu, X. Li, M. Shibayama, U.-i. Chung, T. Sakai, *Macromolecules* **2017**, *50*, 9411.
[12] M. Arifuzzaman, Z. L. Wu, T. Kurokawa, A. Kakugo, J. P. Gong, *Soft Matter* **2012**, *8*, 8060.
[13] H. Kamata, Y. Akagi, Y. Kayasuga-Kariya, U. I. Chung, T. Sakai, *Science* **2014**, *343*, 873.
[14] S. Kim, A. M. Peterson, N. Holten-Andersen, *Chem. Mater.* **2018**, *30*, 3648.
[15] R. Takahashi, Y. Ikura, D. R. King, T. Nonoyama, T. Nakajima, T. Kurokawa, H. Kuroda, Y. Tonegawa, J. P. Gong, *Soft Matter* **2016**, *12*, 5081.
[16] T. Kakuta, Y. Takashima, M. Nakahata, M. Otsubo, H. Yamaguchi, A. Harada, *Adv. Mater.* **2013**, *25*, 2849.
[17] K. Wei, M. Zhu, Y. Sun, J. Xu, Q. Feng, S. Lin, T. Wu, J. Xu, F. Tian, J. XIa, G. Li, L. Bian, *Macromolecules* **2016**, *49*, 866.
[18] G. Marcelo, M. López-González, F. Mendicuti, M. P. Tarazona, M. Valiente, *Macromolecules* **2014**, *47*, 6028.
[19] A. S. Gladman, E. A. Matsumoto, R. G. Nuzzo, L. Mahadevan, J. A. Lewis, *Nat. Mater.* **2016**, *15*, 413.
[20] X. Wang, H. Huang, H. Liu, F. Rehfeldt, X. Wang, K. Zhang, *Macromol. Chem. Phys.* **2019**, *220*, 1800562.
[21] P. Thoniyot, M. J. Tan, A. A. Karim, D. J. Young, X. J. Loh, *Adv. Sci.* **2015**, *2*, 1400010.
[22] Q. Wang, Z. Gao, *J. Mech. Phys. Solids* **2016**, *94*, 127.
[23] Y. Huang, D. R. King, T. L. Sun, T. Nonoyama, T. Kurokawa, T. Nakajima, J. P. Gong, *Adv. Funct. Mater.* **2017**, *27*, 1605350.
[24] T. L. Sun, T. Kurokawa, S. Kuroda, A. B. Ihsan, T. Akasaki, K. Sato, M. A. Haque, T. Nakajima, J. P. Gong, *Nat. Mater.* **2013**, *12*, 932.
[25] A. B. Ihsan, T. L. Sun, S. Kuroda, M. A. Haque, T. Kurokawa, T. Nakajima, J. P. Gong, *J. Mater. Chem. B* **2013**, *1*, 4555.
[26] Y. Tian, T. A. Hatton, K. C. Tam, *Polymer* **2014**, *55*, 3886.
[27] Q. Wang, J. L. Mynar, M. Yoshida, E. Lee, M. Lee, K. Okuro, K. Kinbara, T. Aida, *Nature* **2010**, *463*, 339.
[28] H. Arazoe, D. Miyajima, K. Akaike, F. Araoka, E. Sato, T. Hikima, M. Kawamoto, T. Aida, *Nat. Mater.* **2016**, *15*, 1084.
[29] Z. P. Xu, G. Stevenson, C. Q. Lu, G. Q. Lu, *J. Phys. Chem. B* **2006**, *110*, 16923.